Journal of Power Sources 407 (2018) 31–43

Contents lists available at ScienceDirect

Journal of Power Sources

journal homepage: www.elsevier.com/locate/jpowsour

A review of structural properties and synthesis methods of solid electrolyte materials in the $Li_2S - P_2S_5$ binary system

Ömer Ulaş Kudu[a,b], Theodosios Famprikis[a,c,d], Benoit Fleutot[a,b], Marc-David Braida[e], Thierry Le Mercier[e], M. Saïful Islam[d], Christian Masquelier[a,b,c,*]

[a] Laboratoire de Réactivité et de Chimie des Solides (UMR CNRS 7314), Université de Picardie Jules Verne, 33 rue Saint Leu, 80039, Amiens Cedex, France
[b] Réseau sur le Stockage Électrochimique de l'Énergie (RS2E), FR CNRS 3459, 80039, Amiens, France
[c] ALISTORE European Research Institute, FR CNRS 3104, 80039, Amiens Cedex, France
[d] Department of Chemistry, University of Bath, Bath BA2 7AY, United Kingdom
[e] Solvay R&I, 52 rue de la Haie Coq, 93306, Aubervilliers, France

HIGHLIGHTS

- Structural properties within the Li2S-P2S5 system.
- Possible mechanisms are proposed for the fast ionic conduction observed in glass-ceramics. State-of-the-art in the field.
- Overlooked aspects for application.

ARTICLE INFO

Keywords:
All-solid-state battery
Solid sulfide electrolyte
Li_2S–P_2S_5 binary system
Synthesis
Structure
Stability

ABSTRACT

All-solid-state-batteries (ASSBs) are one of the most promising post-lithium-ion technologies that can increase the specific energy density and safety of secondary lithium batteries. Solid sulfide electrolytes are considered as promising candidates to be used in ASSBs owing to high ionic conductivities. In particular, solid electrolytes in the $Li_2S - P_2S_5$ binary system have attracted considerable attention as they are composed of low-cost elements and they provide ionic conductivity values comparable to those of liquid electrolytes ($> 10^{-4}$ Scm^{-1}). In this review, the structural properties and synthesis methods of materials in the binary system are summarized. Distinctions in local structures and Li-ion conduction properties between glassy, glass-ceramic, and crystalline materials are highlighted. Possible mechanisms are proposed for the fast ionic conduction observed in glass-ceramics. Important parameters of each synthesis method are suggested and the relationships between structure, synthesis and material properties are discussed. The goals of this review are to provide greater understanding of the state-of-the-art in the field, and to point out the overlooked aspects for application.

1. Introduction

The ever rising world energy demand, coupled with the push towards decarbonisation has been straining the current system of energy production and allocation [1]. Notably, the intermittent nature of renewable energy production (predominantly solar and wind, but also geothermal and tidal) necessitates the development of efficient and dependable energy storage [2,3]. Electrochemical energy storage, in the form of batteries and/or fuel cells, is considered the most efficient and mature candidate for energy storage at the medium scale (in the order of kWh for electromobility) and large-scale (in the order of MWh for stationary applications) [4].

Among battery technologies, the rechargeable lithium-ion battery has met unparalleled success for small-scale energy storage (in the order of Wh), as demonstrated by the global use of portable electronics [5]. The success of lithium-ion batteries has been due to their high specific energy density and appropriate cycle-life, currently pushing towards 250 Wh/kg for over 1000 cycles [6]. However, for applications of increasing scale it is not evident that this mature technology can simply be scaled-up to meet demand [7]. This is because of the changing requirement profile for different storage applications. For example, the cost, safety and lifetime requirements become more stringent for

* Corresponding author. Laboratoire de Réactivité et de Chimie des Solides (UMR CNRS 7314), Université de Picardie Jules Verne, 33 rue Saint Leu, 80039, Amiens Cedex, France.
E-mail address: christian.masquelier@u-picardie.fr (C. Masquelier).

https://doi.org/10.1016/j.jpowsour.2018.10.037
Received 10 July 2018; Received in revised form 7 October 2018; Accepted 10 October 2018
Available online 22 October 2018
0378-7753/

higher-scale applications. For stationary energy storage, the volumetric and gravimetric energy densities become less relevant [4]. The changing application requirements have motivated research into alternative battery technologies that could be better adapted to meet these varying requirement profiles [8].

The all-solid-state battery (ASSB) is one of the most promising emerging post-lithium-ion technologies [9]. At the core of the ASSB concept is the replacement of the toxic, flammable organic liquid electrolytes utilized in lithium-ion cells with solid electrolytes. Naturally, such a substitution incurs an intrinsic safer character to ASSBs, which constitutes their major advantage for larger-scale applications [10]. Furthermore, in inorganic solid electrolytes, the unique mobile species are cations (e.g. Li^+ with transference number $t_{Li+} = 1$) which could lead to superior kinetics and allow for high-rate operation with faster charge and discharge [9,11]. Finally, the solid-nature of the electrolyte allows bipolar-stacking cell geometries [12] and possible utilization of metallic Li^0 anodes, which could lead to energy densities surpassing those of the current lithium-ion systems [9].

In this light, it is evident that the development of ASSBs hinges on the development of appropriate solid electrolyte materials, which can enable the manifestation of the above-mentioned benefits. The first requirement for solid electrolytes is, naturally, a high overall ionic conductivity of at least 10^{-4} Scm^{-1} and preferably $> 10^{-3}$ Scm^{-1} at room temperature [13]. In addition, a low activation energy of < 0.4 eV is advantageous, ensuring stable operation at a wider temperature range. Most solid electrolyte materials (and especially the sulfides examined in this short review) are quite unstable in the electrochemical potentials relevant to battery operation (such as 0–4.5 V vs. Li^0) [14]; however this is not strictly prohibitive as due to the solid nature of the ASSB, decomposition can be confined to the interface between electrolyte and electrodes [15]. It is imperative to design solid electrolytes that form favourable interfacial decomposition layers with relevant electrode materials. Namely, the perfect interface would be ionically conductive (i.e. does not block Li^+ diffusion similar to the SEI in a lithium-ion cell) and is as thin as possible (i.e. in the order of nm). The thickness of the interface is in turn controlled by the electronic conductivity of the interface, which, consequently, should be as low as possible to limit the extent of electrochemical decomposition. Finally, the solid electrolyte should be cheap, processed easily and stable at the temperatures relevant to battery operation (e.g. −50 to 150 °C).

Sulfide electrolytes have received a lot of attention owing to their high ionic conductivities ($> 10^{-4}$ Scm^{-1}) [16], and their good contact with electrode materials due to their mechanical softness [17,18]. As shown in Fig. 1, 10–20% of the publications in the literature about

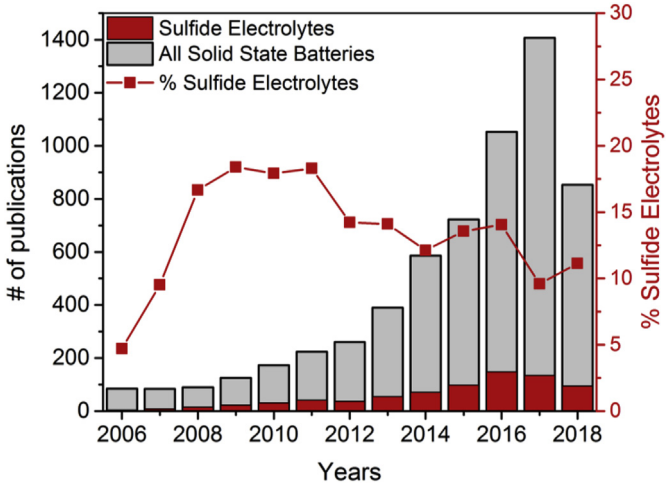

Fig. 1. Number of publications about ASSBs and Sulfide Electrolytes year by year since 2006. The data was gathered from http://scholar.google.com on 22/06/18.

ASSBs were related to the sulfide electrolytes in the last decade. The sulfide electrolytes in the "simple" $Li_2S - P_2S_5$ binary system (LPS family) are particularly interesting as they possess high conductivities ($> 10^{-4}$ Scm^{-1}) without the addition of any extra element (Si, Ge, Al) [19]. Several crystalline and amorphous materials in the LPS family were reported using different synthesis methods.

In this article, we summarize the structural and ionic conduction properties of these materials prepared by different synthesis methods. We highlight the important parameters particularly relevant to each synthesis route and to identify their potential for the up-scaled production of the electrolytes for the next generation of ASSBs.

2. Crystal structures vs. ionic conductivity in the Li_2S–P_2S_5 tie line

As illustrated in Fig. 2, five anionic species are commonly observed in the materials formed within the $Li_2S - P_2S_5$ binary system, summarized as follows:

- Ortho-thiophosphate moieties (isolated $\mathbf{PS_4^{3-}}$ tetrahedra) form the majority of the structure in high quantities of Li_2S (> 75 mol%) [19–27].
- Pyro-thiophosphate moieties ($\mathbf{P_2S_7^{4-}}$), composed of two corner sharing PS_4 tetrahedra, are typically observed in the structure of the compositions with lower quantities of Li_2S (< 75 mol%) [19,20,22,23,28–32].
- Hypo-thiodiphosphate moieties ($\mathbf{P_2S_6^{4-}}$) are basically formed by two PS_3 units with P—P bonding in between. As the only one in the LPS family, the formal oxidation state of the phosphorus in the $P_2S_6^{4-}$ anion is +4, whereas it is +5 for the other moieties.
- Two extra species are observed for the 60 mol% Li_2S composition [19,22]. While the meta-thiodiphosphate moieties ($\mathbf{P_2S_6^{2-}}$) can be visualized as two edge sharing PS_4 units, meta-thiophosphate moieties are described as the polymeric chains of $\mathbf{PS_3^-}$.

Various compositions have been synthesized in the binary system. Glassy materials have been quite popular owing to their decent conductivity values ($> 10^{-5}$ Scm^{-1}) until glass-ceramics were investigated in depth. Initially, glass-ceramic materials were produced by nucleating crystals in an amorphous matrix of ball-milled material, through heat treatment [33]. However, recent studies show that LPS materials crystallized from the melt by slow cooling contain partially amorphous regions [22,34]: this could signify a natural tendency of these materials to exist as glass-ceramic structures.

The differences in the local structures of glassy and glass-ceramic materials were investigated with the help of pair distribution function (PDF) analysis, Raman, and NMR [19,28,35,40] that highlight various quantities and types of structural moieties. As shown in Table 1, a variety of structural units ($P_2S_6^{4}$, $P_2S_7^{4-}$, and PS_4^{3-}) are present in the glassy materials with Li_2S compositions higher than 60 mol%. The relative ratios of these units depend on the initial composition of the material. For each composition, the structural moieties with the greatest content are marked in bold in Table 1. It is noted that the glassy materials with the same composition synthesized by different methods show similar relative ratios of the structural moieties [19,36]. Thus, it can be inferred that a "steady-state" is achieved in the local structure of the glassy materials, where the relative ratios of the anions reach an "equilibrium" and do not change regardless of the synthesis procedure. In contrast to the glassy material of each composition, the types and the relative ratios of structural moieties in each crystalline LPS phase are specific as presented in Table 1. Since glass-ceramics are obtained by nucleating crystals in glassy materials via heat treatment, the relative ratios of the moieties change after the heat treatment of glassy materials.

In the $P_2S_5 - Li_2S$ system, 9 crystal structures have been reported. The ones that are discussed in detail in this review are illustrated in

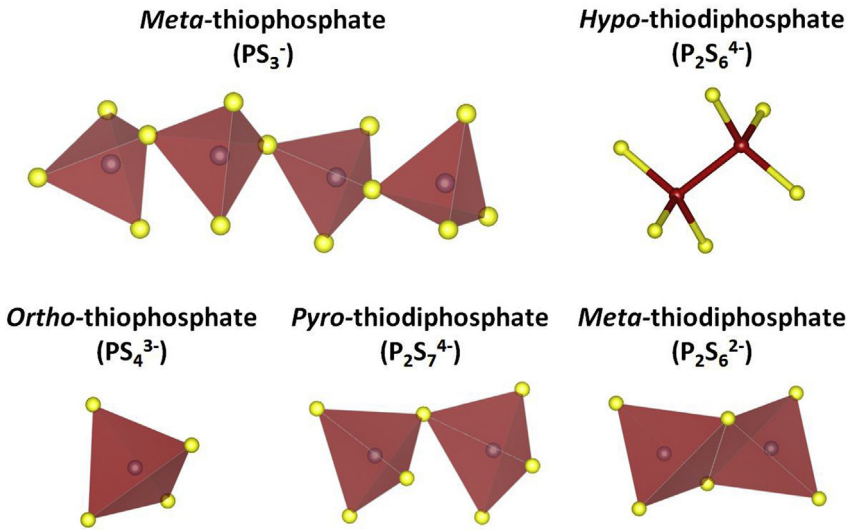

Fig. 2. The anionic species observed in materials. formed within the Li_2S-P_2S_5 binary system.

Table 1
Summary of the crystalline phases and the local structures observed at different compositions. The species with the highest abundance was marked bold in the local structures [19,20,22,23,28,35–40].

Mol% Li_2S	Crystalline phases observed after heat-treatment	Local P−S units in the glass	Local P−S units in the crystal
50	$Li_2P_2S_6$	PS_3^-	$P_2S_6^{2-}$
60	$Li_2P_2S_6$, $Li_4P_2S_6$	$P_2S_6^{2-}$, $P_2S_6^{4-}$, **$P_2S_7^{4-}$**	$P_2S_6^{2-}$, $P_2S_6^{4-}$
67	$Li_4P_2S_6$	$P_2S_6^{4-}$, **$P_2S_7^{4-}$**, PS_4^{3-}	$P_2S_6^{4-}$
70	$Li_7P_3S_{11}$	$P_2S_6^{4-}$, **$P_2S_7^{4-}$**, **PS_4^{3-}**	$P_2S_7^{4-}$, PS_4^{3-}
75	ϒ-Li_3PS_4	$P_2S_6^{4-}$, $P_2S_7^{4-}$, **PS_4^{3-}**	PS_4^{3-}
	β-Li_3PS_4		
	α-Li_3PS_4	–	
	δ-Li_3PS_4	–	
	Thio-lisicon analogue III	–	
80	Li_7PS_6, Li_3PS_4, Li_2S	$P_2S_6^{4-}$, $P_2S_7^{4-}$, **PS_4^{3-}**	PS_4^{3-}
	Thio-lisicon analogue II		
	Thio-lisicon analogue III		

Fig. 3. Table 2 shows the summary of the space groups and the lattice parameters of some of the crystalline samples in the LPS family. In addition to the crystal structures that we discuss, there are also a few studies mentioning "Thio-lisicon analogue II and III" structures, which were observed in glass-ceramic materials with 75, 78 and 80 mol% Li_2S compositions [20,27,41–47]. These phases were reported by *Hayashi* et al. for the first time due to the similarities of their XRD patterns with those of $Li_{4-x}Ge_{1-x}P_xS_4$ compositions reported by *Kanno* et al. [48] (where $0.6 < x < 0.8$ and $0.8 < x < 1.0$ for analogue II and III, respectively). The proposed stoichiometries for the analogues II and III were $Li_{3.25}P_{0.95}S_4$ and $Li_{3.2}P_{0.96}S_4$, respectively. Nevertheless, to our knowledge, they have not been confirmed by any compositional analysis yet. The powder XRD data of the above-mentioned studies show qualitative resemblance to β-Li_3PS_4.

2.1. Crystal structure of $Li_2P_2S_6$

The $Li_2P_2S_6$ stoichiometry corresponds to a 50% Li_2S - 50% P_2S_5 mixture. The crystal structure is described within the monoclinic C2/m space group, the local structure of which being composed of meta-thiodiphosphate groups ($P_2S_6^{2-}$) [22]. Interestingly, polymeric PS_3^- chains present in the amorphous material with 50 mol% Li_2S [36] are not observed in the crystalline material [22]. It can be inferred from these results that the PS_3^- chains break and form isolated $P_2S_6^{2-}$ dimers.

In terms of ionic conductivity, structural and maximum entropy method (MEM) analyses revealed that the conduction occurs only in one-dimension, which is responsible for the low ionic conductivity of 7.8×10^{-11} Scm^{-1} and the relatively high activation energy barrier of around 0.48 eV at room temperature. Hence, this material is not considered as an important solid electrolyte.

2.2. Crystal structure of $Li_4P_2S_6$

The reaction to produce $Li_4P_2S_6$ crystals is unique as its composition is not positioned exactly on the tie line between Li_2S and P_2S_5. It can be obtained from a 67 mol% Li_2S composition, which adds up to the $Li_4P_2S_7$ stoichiometry, following the overall reactions:

$$2\,Li_2S + P_2S_5 = Li_4P_2S_6 + S \text{ or } Li_4P_2S_7 = Li_4P_2S_6 + S$$

It should be emphasized that the local structures of glassy $Li_4P_2S_7$ and crystalline $Li_4P_2S_6$ differ significantly. The main building block of the $Li_4P_2S_7$ glass is $P_2S_7^{4-}$ units [19,23,53] whereas the crystalline $Li_4P_2S_6$ is composed mostly of $P_2S_6^{4-}$ anions [34,49,54]. The $Li_4P_2S_6$ composition is frequently observed as a by-product of the synthesis of the other members of the LPS family. Moreover, the degradation of the metastable phases such as $Li_7P_3S_{11}$ at high temperature leads to the formation of $Li_4P_2S_6$ [28–30,32,41]. These reactions can be attributed to the evaporation of the reagents and to the high stability of the $Li_4P_2S_6$ phase. Indeed, the material was shown to be thermally stable until 950 °C in Ar, and 280 °C in ambient atmosphere (%humidity not specified) [41].

While the space group describing the crystal structure of $Li_4P_2S_6$ was initially reported as being *$P6_3/mcm$* [49], recent studies showed that P-31 m describes the structure more properly, where the $P_2S_6^{4-}$ units are stacked as layers [34,54]. Calculations based on density functional theory showed that the main mechanism of ionic conduction is the vacancy mediated conduction in the Li positions between the $P_2S_6^{4-}$ planes. The low presence of the vacancies leads to a low ionic conductivity (2.9×10^{-11} Scm^{-1}) and the high activation energy (~0.7 eV) [34].

Although the ionic conductivity of $Li_4P_2S_6$ is in the level of 10^{-11} Scm^{-1}, some studies [49,54] report on conductivities in the levels of 10^{-7} – 10^{-6} Scm^{-1}. Recently, *Dietrich* et al. showed that crystalline $Li_4P_2S_6$ can only be synthesized with a glass-ceramic microstructure, where the amorphous part is mainly composed of PS_4^{3-} units [34]. Although the exact reason is not clear, it is known that the formation of

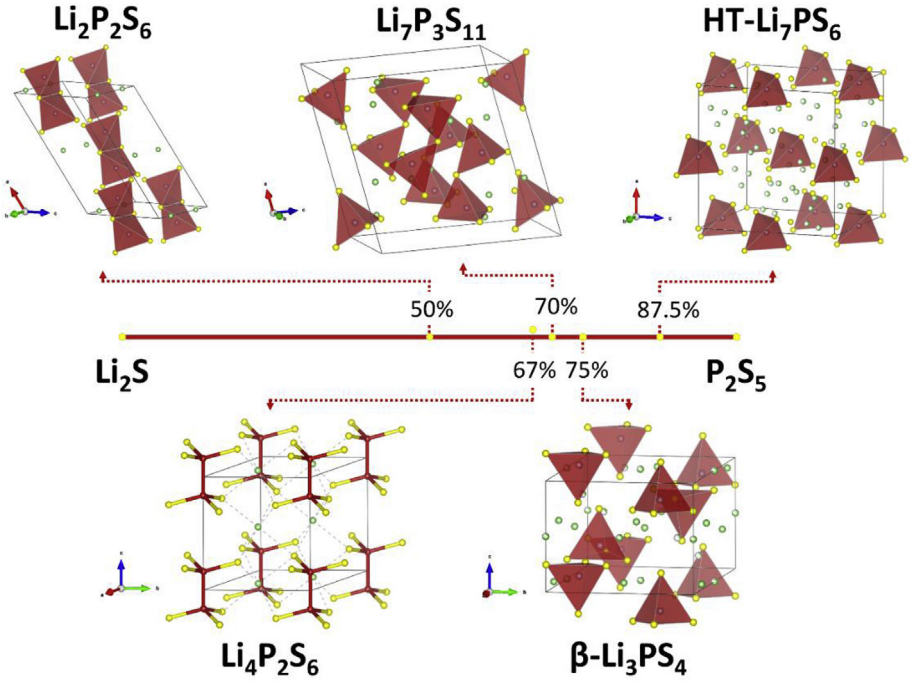

Fig. 3. Some of the crystal structures observed in materials. formed within Li_2S-P_2S_5 binary system.

Table 2
Summary of the crystallographic properties of crystalline materials in the LPS family. Profile parameters of β-Li_3PS_4 obtained by different experimental conditions are given for comparison (SS: Solid-state, MC: Mechano-chemical, WC: Wet chemistry).

Ref	Crystal	Space Group	Synthesis Method	Measur. T. (°C)	Lattice param. (Å)			Lattice angles (°)		
					a	b	C	α	β	ϒ
[22]	**$Li_2P_2S_6$**	C2/m	MC	RT	11.15	7.03	6.55	90.0	125.6	90.0
[34]	**$Li_4P_2S_6$**	P-31 m	SS	RT	6.08	6.08	6.60	90	90	120
[49]	**$Li_7P_3S_{11}$**	P-1	MC	RT	12.50	6.03	12.53	102.9	113.2	74.5
[50]	**β-Li_3PS_4**	Pnma	SS	RT	13.07	8.02	6.10	90.0	90.0	90.0
[51]	**β-Li_3PS_4**	Pnma	SS	**339**	12.82	8.22	6.12	90.0	90.0	90.0
[21]	**β-Li_3PS_4**	Pnma	**WC**	RT	12.99	8.06	6.14	90.0	90.0	90.0
[52]	**LT-Li_7PS_6**	$Pna2_1$	SS	RT	14.08	6.92	9.96	90.0	90.0	90.0
[52]	**HT-Li_7PS_6**	F-43 m	SS	RT	9.99	9.99	9.99	90.0	90.0	90.0

glass-ceramic structures enhances the ionic conductivity of materials in the LPS family [20,33,35,41,55].

2.3. Crystal structure of $Li_7P_3S_{11}$

Crystalline $Li_7P_3S_{11}$ is obtained for the 70% Li_2S – 30% P_2S_5 composition, as an extremely important member of the LPS family due to its very high ionic conductivity (up to 1.7×10^{-2} Scm^{-1} at RT [56]). It is described in the triclinic space group P-1 with a fairly large unit cell (V/Z = 414.7 $Å^3$/unit formula), composed of PS_4^{3-} and $P_2S_7^{4-}$ anions in a 1:1 ratio. Unlike other ionic conductors of the LPS family, it was proposed that the ionic conductivity does not proceed via slow diffusion of isolated defects (i.e. Li^+ vacancies), but rather by collective motion of multiple defects [57]. All lithium sites are tetrahedrally coordinated (LiS_4) and interconnected by further empty tetrahedral sites ($\square S_4$), providing a 3D diffusion pathway with a relatively flat energy profile [57,58]. This is consistent with the observation of Wang, Ceder et al. that the sulfide anion sublattice in $Li_7P_3S_{11}$ approaches a base-centered-cubic close-packing, which should afford the lowest activation energies for conduction among close-packed structures by enabling 3D diffusion solely by tetrahedron-to-tetrahedron hopping [59].

Obtaining a fully crystalline $Li_7P_3S_{11}$ is challenging due to its narrow thermal stability window and it is generally obtained as a glass-ceramic material by annealing glasses between 200 °C and 300 °C for 1–3 h [58,60,61]. In some reports [30,61], a two-step annealing mechanism was suggested to promote nucleation before the growth step. However, the increase in the ionic conductivity was minor. Annealing of the glassy material at a temperature higher than 300 °C leads to partial to complete decomposition, typically to Li_3PS_4, $Li_4P_2S_6$, and S [30,32,40,62]. Likewise, a high temperature (700 °C) synthesis from the reagents leads to the formation of similar side products and low conductivity (2.6×10^{-8} Scm^{-1}) [37]. Nevertheless, such information do not necessarily suggest that the crystal is stable below 300 °C. It was reported that annealing at 300 °C for 10 days also caused similar disproportionation [28].

The high conductivity of crystalline (and glass-ceramic) $Li_7P_3S_{11}$ is very attractive for its use as a solid electrolyte. However, it is noted that obtaining crystalline $Li_7P_3S_{11}$ requires a very precise control of the synthesis and annealing parameters.

2.4. Crystal structures of Li_3PS_4

Li_3PS_4 has a stoichiometry of 75% Li_2S - 25% P_2S_5. Four different crystalline polymorphs have been reported in the literature as the following: **β- Li_3PS_4**, **ϒ- Li_3PS_4**, **α- Li_3PS_4**, and **δ- Li_3PS_4**.

α-Li_3PS_4 crystallizes in an orthorhombic unit-cell within the *Pbcn*

space group [63], obtained at a relatively high temperature (485 °C), and stable until at least 633 °C [51]. **δ-Li_3PS_4**, on the other hand, was obtained at 300 °C and under 5 GPa pressure [64]. The space group of its tetragonal crystalline structure is $P42_1c$. The formation temperature of **ϒ-Li_3PS_4** has not been reported clearly, but it has an orthorhombic crystalline structure in the $Pnm2_1$ space group [51].

The **β-Li_3PS_4** polymorph was named and reported by *Homma* et al. in 2011 [51], after heating the **ϒ-Li_3PS_4** polymorph to 300 °C. A phase transition to form an orthorhombic structure within the *Pnma* space group at high temperature was reported, but **β-Li_3PS_4** crystallized back into the ϒ-Li_3PS_4 polymorph when cooled back to RT. However, *Mercier* et al. reported on the same crystalline structure (*Pnma*) to be stable for Li_3PS_4 at RT [49]. Although the exact reason of the difference is not clear, one possible explanation could be stoichiometric differences between the samples, which originated from the evaporation of the reagents at high temperature (> 500 °C). It was reported that a small change in the stoichiometry of $Li_{3+5x}P_{1-x}S_4$ (x = 0.03) can lead to the stabilization of a crystal structure similar to the β polymorph at RT [65].

The **β** polymorph is described as composed of a hexagonal close packing of sulfide ions, with lithium and phosphorus in the generated interstitials [51]. Phosphorus occupies 1/8 of the tetrahedral sites (Wyckoff 4c), forming isolated PS_4 tetrahedra. Two Li per formula unit are placed in tetrahedral sites (Wyckoff 8d), while the remaining Li is divided between tetrahedral (Wyckoff 4c) and octahedral (Wyckoff 4b) positions. These latter sites form a face-sharing octahedral-tetrahedral chain across the b-axis, which is likely a key feature of Li^+ migration in the crystal. The ratios of octahedral to tetrahedral occupation for Li are reported to range from 0.7:0.3 to 0.41:0.59 [50,51,66,67] and could be dependent on the synthesis method and/or the temperature. The difference in size and bonding character of Li and P induces a distortion in the close-packing arrangement, which actually deviates from perfect hexagonal. The sulfide ions in each layer converge around the smaller P, as expected from the strong covalent P—S bonds, resulting in $V_{PS4} = 4.4$ Å^3 (very close to those observed for PS_4 in $Li_7P_3S_{11}$ [58] and Li_7PS_6 [52]). In contrast, a larger tetrahedral coordination is afforded for the larger, ionically-bonding Li, resulting in $V_{LiS4} = 7.0$ Å^3 and 7.62 Å^3 for 8d and 4c, respectively. It has been suggested that this distortion causes the sulfide close-packing to approach a base-centered-cubic motif with positive consequences for three-dimensional Li^+ migration as discussed for $Li_7P_3S_{11}$ above [59]. This could explain the improved conductivity compared with that of the γ-phase.

Initially, **β-Li_3PS_4** did not receive too much attention due to its low bulk conductivity (2.61×10^{-7} Scm^{-1} at RT) [23]. However, a drastic increase in the conductivity was reported for "nano-porous" β-Li_3PS_4 synthesized via wet-chemistry (1.6×10^{-4} S cm^{-1} with an activation energy of 0.36 eV) [21] and it was discussed that the high conductivity originated from a "surface conduction mechanism". It should also be noted that glassy Li_3PS_4 synthesized by ball-milling yields quite similar conduction properties (2.0×10^{-4} Scm^{-1}, 0.35 eV) [68] to those of the "nano-porous" β-Li_3PS_4. Recent transmission electron microscopy (TEM) observations employing in-situ heating and PDF analysis of ball-milled glassy Li_3PS_4 have suggested that the high conductivity could be a property of the β-Li_3PS_4 glass-ceramic, rather than that of the crystal [35,45,55]. TEM micrographs revealed that although the glassy materials were identified as amorphous by XRD, they actually contained isolated nano-crystallites in the size range of 5–20 nm within the amorphous matrix as illustrated in Fig. 4a and b by *Tsukasaki* et al. [45]. However, the crystalline phase was not identified.

In summary, it remains unclear if the high conductivity originates from the crystalline or amorphous parts of the material. From the literature and the similarities of ionic conduction properties between glassy and glass-ceramic materials, three different conduction mechanisms can be highlighted:

- The high conductivity of the Li_3PS_4 glass-ceramics originates from the high interfacial area between the amorphous matrix and the nano-crystallites [55] (Figure 4c, 2nd path).
- The high conductivity of the Li_3PS_4 glass-ceramic happens through the interconnection between nano-crystallites [45] (Figure 4c, 1st path).
- The high conductivity occurs within the amorphous matrix (Figure 4c, 3rd path).

Although the first two mechanisms indicate that the nano-crystallites are involved in the conductivity, there is no clear evidence suggesting that they have any positive effect. It was shown by electron diffraction and pair distribution function analysis that the increase in the crystallinity of glassy Li_3PS_4 leads to the deterioration in the ionic conductivity [35,55]. Hence, the conduction within the amorphous matrix and the crystals should be decoupled with appropriate techniques such as nuclear magnetic resonance, quasi-elastic neutron scattering and impedance spectroscopy for greater understanding leading to effective manipulation of the structure of these glass-ceramics.

In summary, **glassy Li_3PS_4** synthesized by ball-milling and the β polymorph seem to be the most suitable to be used as solid electrolytes due to their decent ionic conductivity values ($\sim 10^{-4}$ Scm^{-1} at RT). The effects of the crystallization in the glassy matrix on the conductivity and the stability (electrochemical, chemical and thermal) of the material should be investigated in further detail.

2.5. Crystal structure of Li_7PS_6

Crystalline (argyrodite-type) **Li_7PS_6** forms for the 87.5% Li_2S – 12.5% P_2S_5 composition in the binary system. PS_4^{3-} anions were identified via NMR, and the presence of S^{2-} was speculated [36]. Two crystalline polymorphs were reported for Li_7PS_6 [52,69]:

- A low temperature (LT < 210 °C) orthorhombic polymorph, described with the space group $Pna2_1$
- A high temperature (HT > 210 °C) cubic polymorph, described with the space group F-43 m

The ionic conductivity of the LT polymorph was measured as 8×10^{-5} Scm^{-1} at room temperature by *Tatsumisago* et al. [33], but no information was given about the HT polymorph. In a different study, the conductivity of the LT and the HT polymorphs were reported as 1.6×10^{-6} Scm^{-1} at 40 °C and 3×10^{-5} Scm^{-1} at 300 °C, respectively [70]. In the same study, the activation energies for the ionic conductivity of LT and HT polymorphs were reported as 0.16 eV and 0.35 eV, respectively. Crystalline Li_7PS_6 was also observed in glass-ceramic materials with nominal Li_2S molar percentages of 78% and 80%, which had been obtained by annealing ball-milled materials [33,41,44]. It was noted that the increase in the ionic conductivity of these glass-ceramics could be explained by the nucleation of the HT polymorph [33].

There are only few studies on Li_7PS_6 reported in the literature, possibly because it is hard to synthesize with high purity [36] and it exhibits a low bulk ionic conductivity. Nevertheless, crystalline Li_7PS_6 can be observed in glass ceramics of different overall composition, for which it has been proposed to have a positive effect on the ionic conductivity of the material [33,44].

3. Synthesis methods

The high Li^+ conductivity of glasses in the $Li_2S - P_2S_5$ binary system has been investigated since the 1980s [53], and the first crystalline ionic conductors related to Li_3PS_4 and $Li_4P_2S_6$ stoichiometry were discovered by Mercier et al. in 1982 [49,50]. The materials were synthesized via solid state reaction, which remained as the only explored synthesis method for two decades. In 2001, *Hayashi* et al. reported on the mechano-chemical synthesis of glasses in the $Li_2S - P_2S_5$

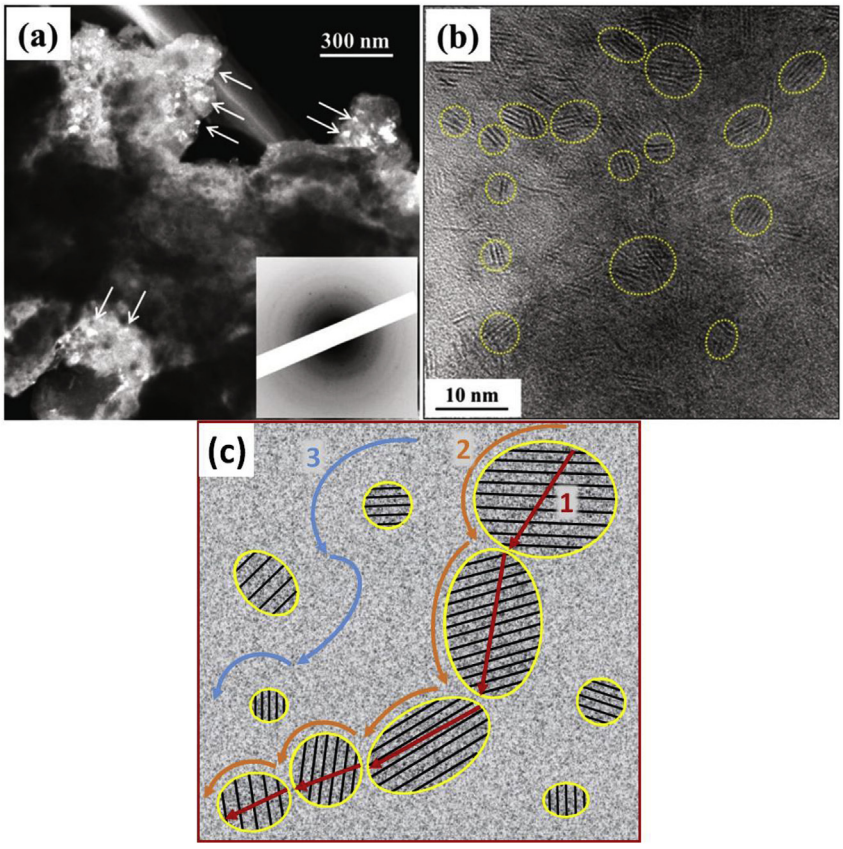

Fig. 4. a) Dark-field image, b) high resolution TEM image (Reprinted with permission from Ref. [45]), and c) schematic illustration of proposed mechanisms of ionic conduction in glass-ceramic materials. Li^+ conduction marked in the 1st path is thorough crystallites in amorphous matrix, the 2nd path is thorough the sites between crystallites and amorphous matrix, and the 3rd path is thorough amorphous matrix.

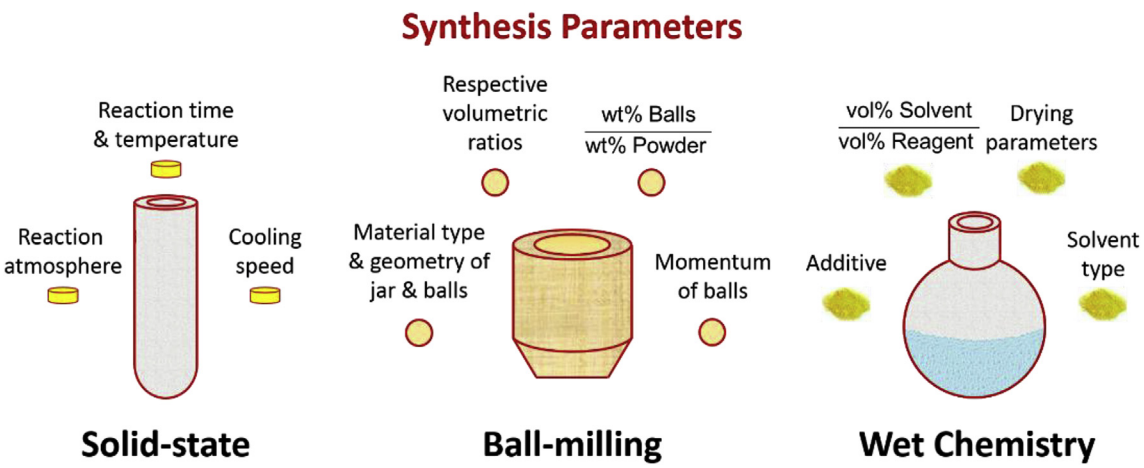

Fig. 5. Important parameters proposed for ball-milling, solid-state route and synthesis via wet chemistry.

binary system for the first time [68]. The use of wet chemistry in the $Li_2S - P_2S_5$ binary system was introduced by *Liu* et al., in 2013 [21], where the reaction of Li_2S and P_2S_5 was mediated by tetrahydrofuran (THF) to form β-Li_3PS_4. Since then, wet chemistry and mechanochemical routes have remained quite popular in the literature. Our selection of important synthesis parameters of different routes are presented in Fig. 5.

In the following sections, the state-of-the-art in terms of synthesis routes gathered from the recent literature, and the ionic conductivity values reached for various types of LPS compositions will be summarized and discussed.

3.1. Solid-state route

The intrinsic nature of "*classical*" solid state reactions requires good solid-solid particle contacts and in some cases parts of the reagent(s) and/or the product(s) are molten at a high temperature to enhance the kinetics of the reactions. The high temperature requirement for the thermodynamics and/or the kinetics of the reactions increases the risk of contamination due to the interaction between the reagents and the reaction vessel. Hence, either an inert or a coated container is used to prevent side-reactions. Nevertheless, the evaporation of the reagents is often observed during the synthesis, which manifests in condensation on the surface of the container after the cooling. Furthermore, in the case of the reactions involving air-sensitive reagents or products, the container should be sealed either in vacuum or inert atmosphere.

Li_3PS_4 and **$Li_4P_2S_6$** were the first crystalline materials reported in the LPS family [49,50]. During the synthesis of both, the reagents were molten in vacuum sealed quartz tubes. Two different approaches were used for cooling:

- Slow cooling to give sufficient time for crystallization
- Quenching the container with ice-water to obtain an amorphous material

Li_3PS_4 was obtained as single crystals using the first method [50]. In the case of the 67% Li_2S – 33% P_2S_5 composition, the melt was quenched to obtain glassy **$Li_4P_2S_7$** [49]. It was explained later that subsequent annealing leads to the formation of crystalline $Li_4P_2S_6$, and sulphur. Additionally it was shown that crystalline $Li_4P_2S_6$ can be obtained by cooling the melt slowly [34,54]. Similarly, the synthesis of **$Li_7P_3S_{11}$ glass-ceramics** requires the formation of an amorphous component in the beginning [56], and the one-step synthesis of crystalline $Li_7P_3S_{11}$ has not been reported yet.

If the formation of a glassy material is not necessary, the reaction can be performed while the reagents are in solid-state [51]. By utilizing this approach in the synthesis of Li_3PS_4, the reaction temperature was reduced from 950 °C to 500 °C; however, the reaction time was increased from 1 h to 5 days [50,51]. It should be noted that the lower temperature values could indeed impede the kinetics of the reaction, but it can enhance the stability of the reaction media and decrease the possibility of the side-reactions. Furthermore, the stability of the container could be enhanced by coating its surface with an inert material. For this reason, carbon-coated quartz tubes are often used for the syntheses [48].

The ionic conductivity and the activation energy values of the materials, which were synthesized by a solid-state route are shown in Table 3. It is noted that the sample preparation could change the conduction properties. Procedures such as changing the applied pressure on the electrolyte pellet during cold pressing, hot pressing the electrolyte and the blocking electrodes, or painting the blocking electrodes on the surfaces of the electrolyte could alter the electrode-electrolyte contact resistances or grain boundary resistance of crystalline materials [56,57]. For example, the effects of hot pressing a $Li_7P_3S_{11}$ glass-ceramic pellet and stainless steel (SS) blocking electrodes on the pellet morphology and resistance were reported by *Seino* et al. [56], as shown in Fig. 6.

In summary, it is noted that this method has not been used frequently in the recent literature, except for the synthesis of crystalline **$Li_4P_2S_6$**. Considering the requirements of sealing the reaction vessel and introducing a quenching step (in some cases), solid-state synthesis does not seem to be a convenient method in terms of scaled-up production.

3.2. 2. mechanochemical route

The mechano-chemical synthesis of LPS materials is generally performed by ball-milling the reagents to obtain an amorphous and/or a crystalline product. The jar and the balls of the ball milling setup are made of an inert and hard material, typically either zirconia, alumina, or silica. During the operation, the movement of the jar transfers the kinetic energy to the balls, which collide with the solid particles inside. The reagent powders initially shape finer particles due to collisions and grinding. Supplying further mechanical energy leads to mechano-chemical reaction.

Understanding the reaction steps is not trivial as the reaction takes place in non-equilibrium conditions and the required time to complete the reaction is dependent on a few parameters such as:

- The material types of the balls, of the jar, and of the reagents
- The respective volumetric ratios of the balls, the jar, and the reagents
- The respective weight ratio of the reagents and the balls
- The geometrical properties of the jar and the balls.
- The momentum of the balls.

Minami and co-workers were the first to report extensively on the use of ball milling for the synthesis of solid electrolytes within the LPS family [68]. In contrast to the solid-state synthesis, it eliminated the necessity of high temperature and quenching operations. As the XRD patterns reported by *Tatsumisago* et al. indicate (see Fig. 7), glassy structures have been reported in the range of 50 mol % < Li_2S < 75 mol%; however, crystalline Li_2S reagent does not get totally amorphized when mol% Li_2S > 75 mol% [33].

Since this first study, the evolution of the parameters of the planetary ball-milling can be summarized as follows:

- Initially, 45 mL alumina jar, 10 balls (10 mm in diameter) with a rotation speed of 370 RPM [68].
- Recently, 45 mL zirconia jar and 500 balls (4 mm in diameter) with a rotation speed of 510 RPM [71,72].

A variety of ball-milling parameters was mentioned above; however, their individual effects have not been studied in detail in the literature. For example, to the best of our knowledge, there is only one comparative study on the nature of the jars and of the balls, and on the size of the balls [73]. Two different materials (zirconia and alumina) were used for the synthesis of $Li_7P_3S_{11-z}$. By keeping the volumes of the jars the same, the material was synthesized in two different conditions:

- The zirconia jar was filled with 500 zirconia balls with the size of 4 mm in diameter, and the rotation speed was fixed at 510 RPM for 8–12 h.
- In the case of the alumina jar, 10 alumina balls with 10 mm diameter were used with 370 RPM speed for 20 h.

As a result, differences were observed in the crystallization temperatures (T_c) of the glasses, and in their ionic conductivities. Although the T_c of the sample synthesized with the alumina setup was lower

Table 3
Summary of the ionic conductivity and the activation energy values of the samples synthesized with the solid state reaction route.

Ref.	Mol% Li2S (Compound)	Annealing T (°C)	Pellet Preparation	Ionic Cond. at RT (Scm-1)	Activation Energy (eV)
[53]	67% ($Li_4P_2S_7$)	–	Annealed at 180 °C	10^{-4}	~0.37
[54]	67% ($Li_4P_2S_6$)	–	Cold pressing	2.38×10^{-7}	0.29
[56]	70% ($Li_7P_3S_{11}$)	–	Cold pressing	8×10^{-5}	–
[56]	70% ($Li_7P_3S_{11}$)	280	Cold pressing	1.4×10^{-3}	0.50
[56]	70% ($Li_7P_3S_{11}$)	280	Densified at 280 °C	1.7×10^{-2}	0.17
[57]	70% ($Li_7P_3S_{11}$)	300	Cold pressing	1.3×10^{-3}	0.21
[57]	70% ($Li_7P_3S_{11}$)	–	SPS sintering	1.2×10^{-2}	0.18
[23]	75% (ϒ-Li_3PS_4)	–	Cold pressing	3×10^{-7}	0.49
[23]	75% (β-Li_3PS_4)	–	Cold pressing	9×10^{-7}	0.46
[51]	75% (ϒ-Li_3PS_4)	–	Annealed at 160 °C	10^{-6}	0.24

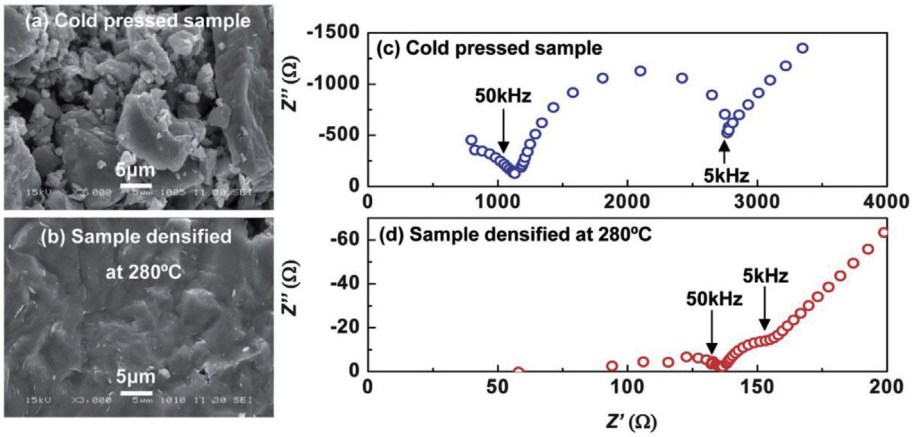

Fig. 6. SEM images of $Li_7P_3S_{11}$ glass-ceramic material from a) cold-pressed sample, b) hot pressed sample (at 94 MPa and 280 °C for 2 h), c) Nyquist plots at −35 °C of c) the cold-pressed sample, and d) the hot pressed sample. Reprinted with permission from Ref. [56].

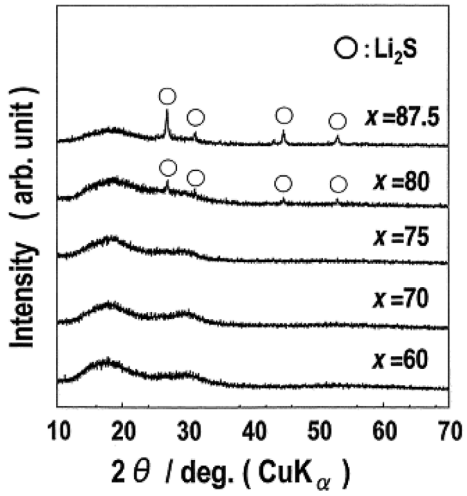

Fig. 7. Powder XRD patterns of xLi2S.(100-x)P2S5 materials synthesized by 20 h of ball-milling. Reprinted with permission from Ref. [33].

(35 °C less), samples synthesized using a zirconia setup yielded a slight increase (less than the double) in the conductivity after annealing.

A different controllable parameter is to introduce periods of rests between ball milling cycles [19,22]. During the operation of ball milling, all the collisions and the friction in the jar generate heat. In some cases, it can cause some side reactions, or slight differences in the stoichiometry due to the evaporation of the reagents. Thus, resting periods are introduced to reduce the temperature in the jar. Typically, ball milling cycles (milling + resting) of 5 + 15 min, or 15 + 15 min have been reported. Nevertheless, the formation of the $P_2S_6^{4-}$ anion cannot be prevented even with the incorporation of the resting period [19,40]. Since the formation of $P_2S_6^{4-}$ requires the loss of a sulphide ion from $P_2S_7^{4-}$, it is not clear if the resting indeed prevents the evaporation of sulphur.

Glassy materials in the LPS family are synthesized using ball-milling at room temperature. The ionic conductivities of these materials can be enhanced by nucleating superionic crystals through subsequent annealing [33,41], the effects of which were discussed in detail for each composition in the chapter on crystal structures. On the other hand, this two-step procedure can be reduced to a one-step one by increasing the ball-milling operation temperature. Indeed, it was reported that increasing the temperature to 55 °C led to the formation of glass-ceramics in the composition region of 70 mol% < Li_2S < 80 mol% [43]. Although ionic conductivities in the range of 10^{-3} Scm^{-1} can be achieved with this one-step reaction, changes in short and long range crystalline order were not investigated, and it could not be reproduced.

To summarize, there are not many variations in the parameters of the ball-milling operation since it was utilized by the group of Minami for the first time and there are no studies to understand how the reaction proceeds during the operation. Recent independent studies report on ball-milled glasses that possess similar local structures, where the quantities of the anion species are in steady-state [19]. More studies are required to reveal the dependency of this equilibrium on the ball milling parameters. The similarities in the structural moieties and in the ionic conductivity values for amorphous materials synthesized by different groups (as shown in Table 4) indicate that ball-milling offers reproducibility and product homogeneity. Ball milling is therefore considered as a reliable technique for up-scaled production. However, it is noted that the ionic conductivities of the glass-ceramics are strongly dependent on the annealing parameters.

3.3. 3. synthesis via wet chemistry

Wet chemistry involves the reaction of reagents in a liquid medium (solvent) and subsequent purification of the compound of interest [74]. Specifically for the LPS system, Li_2S and P_2S_5 precursors can react in the presence of solvents at room temperature to yield the various compounds in the tie-line (Fig. 3). Wet chemistry comes with a variety of controllable parameters such as different solvents, additives and mixing strategies, solvent-to-reagent ratio and drying procedure.

Typically, the solvents utilized are aprotic in order to avoid protonation of the sulfide ion to produce, for example SH^- or $H_xPS_4^{3-x}$ species as well as toxic H_2S gas. Furthermore, the solvents that have been used successfully are (at least moderately) polar, highlighting the active role of the solvent molecules in mediating the reaction. Common polar aprotic solvents utilized in the synthesis of LPS compounds are tetrahydrofuran (THF) [21,75,76], acetonitrile (ACN) [75,77–80] and ethyl acetate (EA) [81].

Despite the recent success of such wet chemical approaches, the reaction mechanism between Li_2S and P_2S_5 in liquid media is not yet well understood. It has been proposed that the electronegative group in the solvent (e.g. ester, ketone or nitrile groups) coordinates to the Li^+ cations, forming $[Li{\cdot}solvent_n]^+$ complexes [81]. The S^{2-} can then attach the P—S—P linkages in P_2S_5 to produce individual thiophosphate moieties such as $P_2S_7^{4-}$ and PS_4^{3-} (Fig. 2). Finally, the anionic and cationic species then typically form a crystalline precipitate that constitutes a co-crystallized complex of the LPS compound and the solvent used: e.g. $Li_3PS_4{\cdot}3THF$ [21], $Li_3PS_4{\cdot}2ACN$ [80]. $Li_3PS_4{\cdot}DME$ [82]. The conductivities of the LPS-solvent complexes are quite low, most likely because Li^+ in these structures is coordinated very strongly by both the thiophosphate anions and the polar solvents, such as the PS_4^{3-} and the

Table 4
Summary of the ionic conductivity and activation energy values of samples synthesized through mechanochemical synthesis.

Ref.	Mol% Li2S (Compound)	Annealing T (°C)	Pellet Preparation	Ionic Cond. at RT (S.cm-1)	Activation Energy (eV)
[33]	60%	–	Cold pressing	8×10^{-6}	0.42
[19]	60%	–	Cold pressing	2×10^{-6}	0.54
[19]	67% ($Li_4P_2S_7$)	–	Cold pressing	3×10^{-5}	0.44
[68]	70% ($Li_7P_3S_{11}$)	–	Cold pressing	4×10^{-5}	0.41
[19]	70% ($Li_7P_3S_{11}$)	–	Cold pressing	3×10^{-5}	0.45
[20]	70% ($Li_7P_3S_{11}$)	300	Cold pressing	3.2×10^{-3}	0.12
[60]	70% ($Li_7P_3S_{11}$)		Cold pressing	5×10^{-5}	0.38
[60]	70% ($Li_7P_3S_{11}$)	250–260	Sintered at 250 °C	2×10^{-3}	0.40
[30]	70% ($Li_7P_3S_{11}$)	–	Cold pressing	8.1×10^{-5}	0.43
[30]	70% ($Li_7P_3S_{11}$)		Hot p. (210–250 °C)	8.6×10^{-3}	0.29
[73]	70% ($Li_7P_3S_{11-z}$)	280	Cold pressing	5.4×10^{-3}	–
[68]	75% (Li_3PS_4)	–	Cold pressing	2×10^{-4}	0.35
[19]	75% (Li_3PS_4)	–	Cold pressing	2×10^{-4}	0.39
[41]	75% (Li_3PS_4)	240	Cold pressing	2.8×10^{-4}	–
[55]	75% (β-Li_3PS_4)	–	Cold pressing	5.9×10^{-4}	–
[55]	75% (β-Li_3PS_4)	120	Cold pressing	7.6×10^{-4}	–
[44]	78%	–	Cold pressing	3.2×10^{-4}	–
[44]	78%	170–240	Cold pressing	1.8×10^{-3}	0.31
[68]	80%	–	Cold pressing	1×10^{-4}	0.36
[19]	80%		Cold pressing	1×10^{-4}	0.44
[33]	80%	215	Cold pressing	6×10^{-4}	0.29
[41]	80%	230		7.2×10^{-4}	–
[68]	87.5% (Li_7PS_6)	–	Cold pressing	1×10^{-5}	0.49

ether group in DME in Li_3PS_4·DME [82].

Solvent-based reactions to form LPS compounds do not proceed to completion as indicated from remaining reagents in the product-solvent mixture. This could be due to partial solubility of the target compound and/or formation of byproducts such as polysulfide species or solvent decomposition products. This is supported by the observation of coloring in the solutions during reaction, e.g. yellow for THF and light blue for ACN [75]. However, it is believed that the majority of such side products are soluble and, as such, the solid precipitate can be washed with excess fresh solvent to ensure purity. Nevertheless, this tendency to form side-products underlines the necessity for reagent purity and especially for completely anhydrous solvents (< 10 ppm H_2O). After washing, the precipitate can be obtained by simple filtration or decanting.

After precipitation, co-crystallized solvent molecules need to be removed in order to obtain the pure LPS compound of interest. This is most often achieved by heating under vacuum; the required temperature depending on the volatility and polarity of the solvent ranging e.g. from 80 °C for THF [83] to 250 °C for DME [84]. It is not evident if all organic species can be removed or a small quantity remains.

It has been proposed that the evaporation of solvent molecules produces unique nano-porous micro-structures, which could be beneficial for ionic conduction. Specifically, in the case of Li_3PS_4, the crystallization of the β-polymorph is observed, with a room-temperature conductivity of up to 3.3×10^{-4} Scm^{-1} depending on the solvent and procedure (see Table 5). We note that these values are several orders of magnitude higher than those observed for the analogues produced by solid-state routes ($\sim 10^{-7}$ Scm^{-1}, see Table 3) and comparable to the high conductivities of ball-milled glasses and (glass-) ceramics ($\sim 10^{-4}$ Scm^{-1}, see Table 4).

Wet chemical routes could possess distinct advantages pertaining to all-solid-state battery integration; namely, the possibility to form intimate contacts of high surface coverage by direct precipitation on electrode materials and/or very thin “separator” membranes [74]. The former has been manifested in attempts to deposit Li_3PS_4 directly on Li^0 to be used as a protected anode [86–88]. The latter has been demonstrated recently to allow the fabrication of self-standing Li_3PS_4 membranes of sub-micron thicknesses (400 nm) [75]. Furthermore, the mesostructure (i.e. μm-scale morphology) of the LPS particles can be tuned by controlling the solvent type. This effect is probably linked to the differences in complexation of Li^+ by the different solvents as well as the symmetry of the resulting LPS solvent co-crystalline complex and the different morphologies reported so far are demonstrated in Fig. 8.

The studies about the reaction mechanism of **$Li_7P_3S_{11}$** in liquid media revealed that the reaction pathway is different than that of Li_3PS_4 [32,62]. It was shown that the mixing of the solvent and the reagents (70 mol% Li_2S – 30 mol% P_2S_5) initially led to the formation of **Li_3PS_4:solvent** and **Li_2S:P_2S_5:solvent** (estimated ratio of Li_2S:P_2S_5 was 1:1) complexes. The reaction to produce $Li_7P_3S_{11}$ glass-ceramic was completed during the following drying process. Interestingly, *M. Calpa*

Table 5
Summary of ionic conductivity and activation energy values for the samples synthesized with the wet chemistry.

Ref.	Mol% Li2S (Compound)	Solvent	Drying Temperature (°C)	Ionic Cond. at RT (S.cm-1)	Activation Energy (eV)
[84]	70% ($Li_7P_3S_{11}$)	DME	250	2.7×10^{-4}	0.39
[32]	70% ($Li_7P_3S_{11}$)	Acetonitrile	260	8.7×10^{-4}	0.37
[62]	70% ($Li_7P_3S_{11}$)	Acetonitrile	220	1.1×10^{-5}	–
[62]	74% ($Li_7P_3S_{11}$)	Acetonitrile	220	1.0×10^{-3}	0.13
[21]	75% (β-Li_3PS_4)	THF	140	1.6×10^{-4}	0.36
[89]	75% (Li_3PS_4)	NMF & n-hexane	180	2.3×10^{-6}	0.47
[80]	75% (β-Li_3PS_4)	Acetonitrile	200	1.2×10^{-4}	0.36
[25]	75% (Li_3PS_4)	EA	160	3.3×10^{-4}	0.32
[90]	75% (Li_3PS_4)	DMC	190	6.4×10^{-6}	0.62
[27]	75% (Li_3PS_4)	EP	170	2.0×10^{-4}	0.43
[83]	75% (β-Li_3PS_4)	THF	140	1.3×10^{-4}	0.27
[81]	75% (Li_3PS_4)	MPK	160	3.0×10^{-7}	–

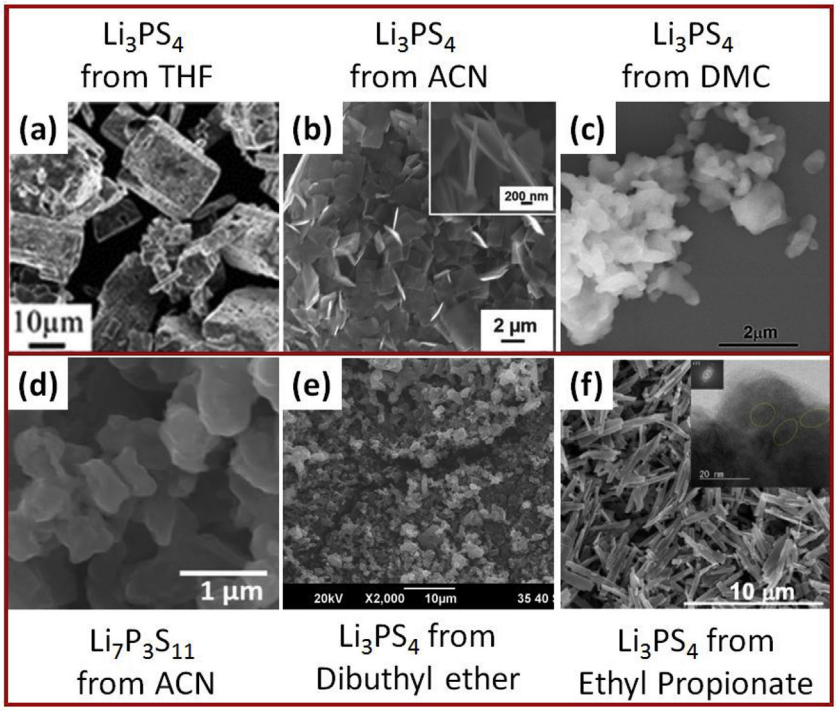

Fig. 8. Micrographs of the diverse meso-structures achievable by wet chemical routes for the synthesis of LPS compounds: (a) orthorhombic 10–30 μm Li_3PS_4 particles from THF [21], (b) square 80-nm-thin Li_3PS_4 nano-platelets ca. 3 μm from ACN [75], (c) agglomerates of irregular 100–500 nm Li_3PS_4 particles from dimethyl carbonate [85], (d) agglomerates of irregular ca. 500-nm $Li_7P_3S_{11}$ particles from ACN [78], (e) irregular 2–3 nm Li_3PS_4 particles from dibutylether [46], and (f) 3 μm by 500 nm by 100–200 nm Li_3PS_4 plates by ethyl propionate [27]. Reprinted with permission from Refs. [21,27,46,75,78,85].

et al. [62] reported that a change in the initial Li_2S content (from 70% to 74 mol%) increased the ionic conductivity of the product from 10^{-5} to 10^{-3} Scm^{-1}. These findings emphasize the necessity of thoroughly understanding how the reaction proceeds to synthesize a solid electrolyte with a high ionic conductivity.

In summary, wet synthesis offers a range of tuneable parameters such as the type and the quantity of solvent(s), mixing strategies, additives and drying procedures. However, up to now only a few studies have attempted to understand of the reaction mechanisms involved. A variety of ionic conductivity and activation energy values have been reported; however, no concrete reason for the differences has been established. More studies are needed to understand the origin of the difference: organic remnants and micro/meso-structural differences could be responsible for the lower conductivity values in some cases, as compared to the products of other synthesis methods (see Tables 3–5).

4. Summary and future outlook

Sulfide electrolytes are good candidates to be used as electrolytes in ASSBs owing to their high ionic conductivities and soft mechanical properties. The LPS family, in particular, has received a considerable amount of attention as it can provide a high Li-ion conductivity without contribution of a transition metal. In this review, structural characteristics of glassy and crystalline materials, and the strengths and weaknesses of different synthesis methods were summarized. Ionic conduction properties as a function of synthesis parameters were tabulated.

Fig. 9 summarizes the interlinked relationships between synthesis, structure and material properties. As discussed in the previous chapters, a variety of structures can be obtained from different synthesis methods. The most interesting structures obtained by different synthesis can be specified as the following:

- Crystals bigger than a few hundred nanometers can be produced by cooling the molten product slowly after solid state synthesis [23].
- Glass-ceramic materials, which are composed of nano-crystallites distributed in their amorphous matrices, can be synthesized via ball-milling [55].
- Nano-crystalline materials can be synthesized via wet chemistry [21].

The structures obtained by different synthesis methods determine the properties of the material. Considering the criteria for a good electrolyte for ASSBs, the properties can be categorized in three sections: Ionic conduction properties, chemical and electrochemical stabilities.

In terms of ionic conduction properties, the structures of the materials play an important role in the conductivity mechanism. For example, in the case of 70 mol% Li_2S – 30 mol% P_2S_5 stoichiometry, crystallization of glassy $Li_7P_3S_{11}$ increases the ionic conductivity [56] from 8×10^{-5} Scm^{-1} to 1.4×10^{-3} Scm^{-1} owing to the 3D conduction pathways forming with the crystalline structure [57]. High conductivity, however, does not always originate from the crystalline phase for all the materials in the LPS family. DFT calculations show that the conductivity of crystalline $Li_4P_2S_6$ can be enhanced drastically with the contribution of an amorphous component (from 2.9×10^{-11} to 10^{-6} Scm^{-1} at RT) [34]. Similarly, the ionic conductivity value for a glass-ceramic Li_3PS_4 material (with β polymorph, 7.5×10^{-4} Scm^{-1}) [55] is significantly higher than the value of the bulk crystalline material (β polymorph, 9×10^{-7} Scm^{-1}) at RT [23]. While there are hypotheses about the reason of the increased conductivity in glass-ceramics, nano-crystalline β-Li_3PS_4 synthesized via wet chemistry offers a decent ionic conductivity value (1.6×10^{-4} Scm^{-1} at RT). Although the mechanisms of conduction are not well understood, it is evident that the high conductivity could be achieved with various types of structures. In particular, crystalline $Li_7P_3S_{11}$, nano-porous β-Li_3PS_4, and glass-ceramic β-Li_3PS_4 materials are promising ($\sigma > 10^{-4}$ Scm^{-1}).

From the chemical stability point of view, the stability in air and in contact with lithium metal anode should be considered separately. However, to the best of our knowledge, there is no comparative study about similar materials synthesized by different methods. Regarding the stability in air, there is only one comparative study by *Muramatsu* et al., in which the chemical stabilities of the glasses with different stoichiometries (synthesized by ball-milling) were compared by observing the H_2S evolution in ambient atmosphere [91]. The quantity of the H_2S evolution was lowest in the case of the Li_3PS_4 glass, which slightly increased after the formation of glass-ceramic material (with thio-lisicon

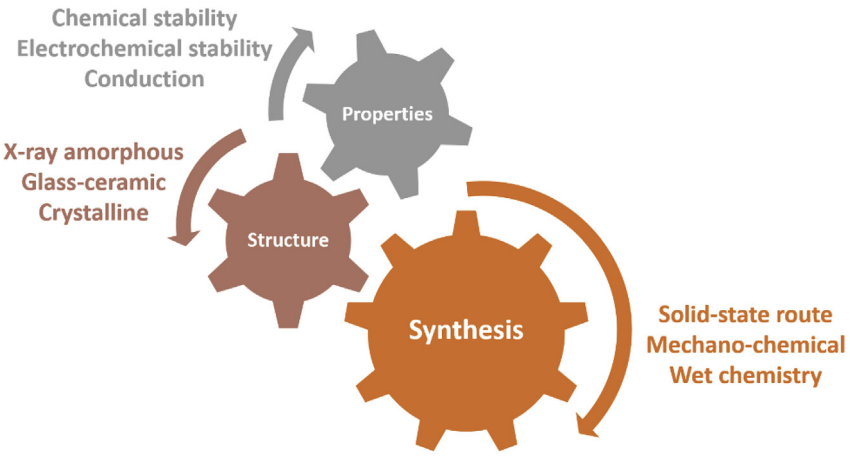

Fig. 9. Schematic image of the interconnection between synthesis, structure and material properties.

analogue III phase) by annealing. Hence, it is inferred that the chemical stability is dependent on the composition and the structure.

At the same time, the potential window and the electrochemical stability of a solid electrolyte are key factors for application in ASSBs. There is a number of methods to assess these properties [26,92,93], among which cyclic voltammetry (CV) is the most widely used [21,42,56,65]. The measurement is generally performed by placing the electrolyte between Li metal (or Li—In alloy) and a blocking electrode (i.e. Pt, Ti, SS). It is noted, however, that this kind of setup could provide misleading information about the electrochemical stability of the LPS electrolytes. For example, the oxidation stability of two Li_3PS_4 samples with the same phase has contradictory results from two different studies (< 3.0 V vs > 5.0 V vs Li/Li^+, respectively), where similar setups were used as described above [27,94]. The difference in the oxidation potentials could be due to the applied scan rate ($20\ mVs^{-1}$ vs $5\ mVs^{-1}$, respectively) or the sample preparation. Thus, a standardization is required for the determination of the electrochemical stability of the electrolytes in order to compare the stability of different phases and compositions. In our opinion, the stability could only be revealed if CV is performed with a low scan rate ($< 1\ mVs^{-1}$), which is low enough to reveal potentially sluggish side reactions. Furthermore, a specific cell configuration utilizing a composite of the solid electrolyte and carbon can help to enhance the observed current signal [95,96]. In this configuration, the solid electrolyte is sandwiched between a pseudo-composite working electrode (e.g. 90 wt% solid electrolyte +10 wt% carbon conductor additive) and a lithium-indium counter electrode (or lithium electrode depending on the chemical stability of the electrolyte). The mixture of solid electrolyte with carbon allows an electronic percolation through the full working electrode and a good evaluation of the electrochemical stability of the electrolyte close to a future composite electrode configuration.

It is evident that the literature has been focused mostly on achieving high ionic conductivity values. However, chemical and electrochemical stability properties are crucial for the application in ASSBs. Similarly, properties of a good synthesis method are also over-looked. Feasibility, up-scalability, and non-toxicity are important properties for the production at industrial scale. Solid-state synthesis is considered to be not feasible in large scale production due to the requirement of sealing and quenching steps. Mechano-chemical and wet chemistry routes are more promising in terms of up-scalability due to the product homogeneity and reproducibility. Furthermore, considering that the electrodes in ASSBs require a good particle contact with the electrolyte, both methods present opportunities for good mixing with the electrode materials. It is possible to prepare electrode-electrolyte mixtures through ball-milling, which is advantageous for the production of mixed cathode materials. An intimate contact between electrode-electrolyte can also be established by coating the electrodes directly with electrolyte using wet chemistry. Nevertheless, issues such as product recovery after ball-milling, and recycling of the solvents after synthesis with soft chemistry remains under consideration.

In summary, even though $Li_2S - P_2S_5$ based solid electrolytes come with limitations in terms of chemical and electrochemical stabilities, they are promising candidates for the next generation of ASSBs owing to their high ionic conductivities ($> 10^{-4}\ Scm^{-1}$). To tackle the limitations properly, stabilities of materials should be assessed in a rigorous manner. Nevertheless, it is not rigorous enough to claim that one synthesis method is more preferable than the other before dependence of different synthesis methods on material properties are examined thoroughly.

Acknowledgements

This work was supported by the Association Nationale de la Recherche et de la Technologie [CIFRE number 2016/1450] and by the ALISTORE-ERI. The authors gratefully thank Dr. Virginie Viallet, who initiated the project, for fruitful discussions.

References

[1] J.B. Goodenough, M.H. Braga, Batteries for electric road vehicles, Dalton Trans. (2017), https://doi.org/10.1039/C7DT03026F.
[2] S. Chu, Y. Cui, N. Liu, The path towards sustainable energy, Nat. Mater. 16 (2017) 16–22, https://doi.org/10.1038/nmat4834.
[3] P.G. Bruce, B. Scrosati, J.M. Tarascon, Nanomaterials for rechargeable lithium batteries, Angew. Chem. Int. Ed. 47 (2008) 2930–2946, https://doi.org/10.1002/anie.200702505.
[4] Z. Yang, J. Zhang, M.C.W. Kintner-Meyer, X. Lu, D. Choi, J.P. Lemmon, J. Liu, Electrochemical energy storage for green grid, Chem. Rev. 111 (2011) 3577–3613, https://doi.org/10.1021/cr100290v.
[5] C. Masquelier, Solid electrolytes: lithium ions on the fast track, Nat. Mater. 10 (2011) 649–650, https://doi.org/10.1038/nmat3105.
[6] X. Han, M. Ouyang, L. Lu, J. Li, Y. Zheng, Z. Li, A comparative study of commercial lithium ion battery cycle life in electrical vehicle: aging mechanism identification, J. Power Sources 251 (2014) 38–54, https://doi.org/10.1016/j.jpowsour.2013.11.029.
[7] P.G. Bruce, S.A. Freunberger, L.J. Hardwick, J.M. Tarascon, Li–O2 and Li–S batteries with high energy storage, Nat. Mater. 11 (2011), https://doi.org/10.1038/nmat3237 172–172.
[8] T. Placke, R. Kloepsch, S. Dühnen, M. Winter, Lithium ion, lithium metal, and alternative rechargeable battery technologies: the odyssey for high energy density, J. Solid State Electrochem. 21 (2017) 1939–1964, https://doi.org/10.1007/s10008-017-3610-7.
[9] J. Janek, W.G. Zeier, A solid future for battery development, Nat. Energy. 1 (2016), https://doi.org/10.1038/nenergy.2016.141.
[10] T. Inoue, K. Mukai, Are all-solid-state lithium-ion batteries really safe?–verification by differential scanning calorimetry with an all-inclusive microcell, ACS Appl. Mater. Interfaces 9 (2017) 1507–1515, https://doi.org/10.1021/acsami.6b13224.
[11] Y. Kato, S. Hori, T. Saito, K. Suzuki, M. Hirayama, A. Mitsui, M. Yonemura, H. Iba, R. Kanno, High-power all-solid-state batteries using sulfide superionic conductors, Nat. Energy. 1 (2016) 16030, https://doi.org/10.1038/nenergy.2016.30.
[12] Y.-S. Hu, Batteries: getting solid, Nat. Energy. 1 (2016), https://doi.org/10.1038/

nenergy.2016.42.
[13] J.C. Bachman, S. Muy, A. Grimaud, H.H. Chang, N. Pour, S.F. Lux, O. Paschos, F. Maglia, S. Lupart, P. Lamp, L. Giordano, Y. Shao-Horn, Inorganic solid-state electrolytes for lithium batteries: mechanisms and properties governing ion conduction, Chem. Rev. 116 (2016) 140–162, https://doi.org/10.1021/acs.chemrev.5b00563.
[14] W.D. Richards, L.J. Miara, Y. Wang, J.C. Kim, G. Ceder, Interface stability in solid-state batteries, Chem. Mater. 28 (2016) 266–273, https://doi.org/10.1021/acs.chemmater.5b04082.
[15] A.C. Luntz, J. Voss, K. Reuter, Interfacial challenges in solid-state Li ion batteries, J. Phys. Chem. Lett. 6 (2015) 4599–4604, https://doi.org/10.1021/acs.jpclett.5b02352.
[16] S. Chen, D. Xie, G. Liu, J.P. Mwizerwa, Q. Zhang, Y. Zhao, X. Xu, X. Yao, Sulfide solid electrolytes for all-solid-state lithium batteries: structure, conductivity, stability and application, Energy Storage Mater 14 (2018) 58–74, https://doi.org/10.1016/j.ensm.2018.02.020.
[17] Z. Deng, Z. Wang, I.-H. Chu, J. Luo, S.P. Ong, Elastic properties of alkali superionic conductor electrolytes from first principles calculations, J. Electrochem. Soc. 163 (2016) A67–A74, https://doi.org/10.1149/2.0061602jes.
[18] A. Sakuda, A. Hayashi, M. Tatsumisago, Sulfide solid electrolyte with favorable mechanical property for all-solid-state lithium battery, Sci. Rep. 3 (2013) 2261, https://doi.org/10.1038/srep02261.
[19] C. Dietrich, D. Weber, S.J. Sedlmaier, S. Indris, S. Culver, D. Walter, J. Janek, W. Zeier, Lithium ion conductivity in Li2S-P2S5 glasses – building units and local structure evolution during the crystallization of the superionic conductors Li3PS4 , Li7P3S11 and Li4P2S6, J. Mater. Chem. A (2017), https://doi.org/10.1039/C7TA06067J.
[20] F. Mizuno, A. Hayashi, K. Tadanaga, M. Tatsumisago, High lithium ion conducting glass-ceramics in the system Li2S-P2S5, Solid State Ionics 177 (2006) 2721–2725, https://doi.org/10.1016/j.ssi.2006.04.017.
[21] Z. Liu, W. Fu, E.A. Payzant, X. Yu, Z. Wu, N.J. Dudney, J. Kiggans, K. Hong, A.J. Rondinone, C. Liang, Anomalous high ionic conductivity of nanoporous β-Li3PS4, J. Am. Chem. Soc. 135 (2013) 975–978, https://doi.org/10.1021/ja3110895.
[22] C. Dietrich, D.A. Weber, S. Culver, A. Senyshyn, S.J. Sedlmaier, S. Indris, J. Janek, W.G. Zeier, Synthesis, structural characterization, and lithium ion conductivity of the lithium thiophosphate Li2P2S6, Inorg. Chem. 56 (2017) 6681–6687, https://doi.org/10.1021/acs.inorgchem.7b00751.
[23] M. Tachez, J. Malugani, R. Mercier, R. Guy, Ionic conductivity of and phase transition in Li thiophosphate Li3PS4, Solid State Ionics 14 (1984) 181–185, https://doi.org/10.1016/0167-2738(84)90097-3.
[24] M. Gobet, S. Greenbaum, G. Sahu, C. Liang, Structural evolution and li dynamics in nanophase Li3PS 4 by solid-state and pulsed-field gradient NMR, Chem. Mater. 26 (2014) 3558–3564, https://doi.org/10.1021/cm5012058.
[25] N.H.H. Phuc, M. Totani, K. Morikawa, H. Muto, A. Matsuda, Preparation of Li3PS4 solid electrolyte using ethyl acetate as synthetic medium, Solid State Ionics 288 (2015) 240–243, https://doi.org/10.1016/j.ssi.2015.11.032.
[26] R. Koerver, F. Walther, I. Aygün, J. Sann, C. Dietrich, W. Zeier, J. Janek, Redox-active cathode interphases in solid-state batteries, J. Mater. Chem. A (2017) 22750–22760, https://doi.org/10.1039/C7TA07641J.
[27] N.H.H. Phuc, K. Morikawa, T. Mitsuhiro, H. Muto, A. Matsuda, Synthesis of plate-like Li3PS4 solid electrolyte via liquid-phase shaking for all-solid-state lithium batteries, Ionics 4 (2017) 1–7, https://doi.org/10.1007/s11581-017-2035-8.
[28] Y. Seino, M. Nakagawa, M. Senga, H. Higuchi, K. Takada, T. Sasaki, Analysis of the structure and degree of crystallisation of 70Li2S–30P2S5 glass ceramic, J. Mater. Chem. A. 3 (2015) 2756–2761, https://doi.org/10.1039/C4TA04332D.
[29] Y. Aoki, K. Ogawa, T. Nakagawa, Y. Hasegawa, Y. Sakiyama, T. Kojima, M. Tabuchi, Chemical and structural changes of 70Li2S-30P2S5 solid electrolyte during heat treatment, Solid State Ionics 310 (2017) 50–55, https://doi.org/10.1016/j.ssi.2017.08.006.
[30] M.R. Busche, D.A. Weber, Y. Schneider, C. Dietrich, S. Wenzel, T. Leichtweiss, D. Schröder, W. Zhang, H. Weigand, D. Walter, S.J. Sedlmaier, D. Houtarde, L.F. Nazar, J. Janek, In situ monitoring of fast Li-ion conductor Li7P3S11 crystallization inside a hot-press setup, Chem. Mater. 28 (2016) 6152–6165, https://doi.org/10.1021/acs.chemmater.6b02163.
[31] R.C. Xu, X.H. Xia, Z.J. Yao, X.L. Wang, C.D. Gu, J.P. Tu, Preparation of Li7P3S11 glass-ceramic electrolyte by dissolution-evaporation method for all-solid-state lithium ion batteries, Electrochim. Acta 219 (2016) 235–240, https://doi.org/10.1016/j.electacta.2016.09.155.
[32] Y. Wang, D. Lu, M. Bowden, P.Z. El Khoury, K.S. Han, Z.D. Deng, J. Xiao, J.-G. Zhang, J. Liu, Formation mechanism of Li7P3S11 solid electrolytes through liquid phase synthesis, Chem. Mater. (2018), https://doi.org/10.1021/acs.chemmater.7b04842 acs.chemmater.7b04842.
[33] M. Tatsumisago, S. Hama, A. Hayashi, H. Morimoto, T. Minami, New lithium ion conducting glass-ceramics prepared from mechanochemical Li2S-P2S5 glasses, Solid State Ionics 154 (2002) 635–640, https://doi.org/10.1016/S0167-2738(02)00509-X.
[34] C. Dietrich, M. Sadowski, S. Sicolo, D.A. Weber, S.J. Sedlmaier, K.S. Weldert, S. Indris, K. Albe, J. Janek, W.G. Zeier, Local structural investigations, defect formation, and ionic conductivity of the lithium ionic conductor Li4P2S6, Chem. Mater. 28 (2016) 8764–8773, https://doi.org/10.1021/acs.chemmater.6b04175.
[35] S. Shiotani, K. Ohara, H. Tsukasaki, S. Mori, R. Kanno, Pair distribution function analysis of sulfide glassy electrolytes for all-solid-state batteries: understanding the improvement of ionic conductivity under annealing condition, Sci. Rep. 7 (2017), https://doi.org/10.1038/s41598-017-07086-y.
[36] H. Eckert, Z. Zhang, J.H. Kennedy, Structural transformation of non-oxide chalcogenide glasses. The short-range order of Li2S-P2S5 glasses studied by quantitative 31P and 6,7Li high-resolution, Chem. Mater. 2 (1990) 273–279, https://doi.org/10.1021/cm00009a017.
[37] F. Mizuno, A. Hayashi, K. Tadanaga, M. Tatsumisago, New, highly ion-conductive crystals precipitated from Li2S-P2S5 glasses, Adv. Mater. 17 (2005) 918–921, https://doi.org/10.1002/adma.200401286.
[38] K. Mori, T. Ichida, K. Iwase, T. Otomo, S. Kohara, H. Arai, Y. Uchimoto, Z. Ogumi, Y. Onodera, T. Fukunaga, Visualization of conduction pathways in lithium superionic conductors: Li2S-P2S5 glasses and Li7P3S11 glass-ceramic, Chem. Phys. Lett. 584 (2013) 113–118, https://doi.org/10.1016/j.cplett.2013.08.016.
[39] K. Ohara, A. Mitsui, M. Mori, Y. Onodera, S. Shiotani, Y. Koyama, Y. Orikasa, M. Murakami, K. Shimoda, K. Mori, T. Fukunaga, H. Arai, Y. Uchimoto, Z. Ogumi, Structural and electronic features of binary Li2S-P2S5 glasses, Sci. Rep. 6 (2016) 21302, https://doi.org/10.1038/srep21302.
[40] Y. Aoki, K. Ogawa, T. Nakagawa, Y. Hasegawa, Y. Sakiyama, T. Kojima, M. Tabuchi, Chemical and structural changes of 70Li2S-30P2S5 solid electrolyte during heat treatment, Solid State Ionics 310 (2017) 50–55, https://doi.org/10.1016/j.ssi.2017.08.006.
[41] A. Hayashi, S. Hama, T. Minami, M. Tatsumisago, Formation of superionic crystals from mechanically milled Li2S-P2S5 glasses, Electrochem. Commun. 5 (2003) 111–114, https://doi.org/10.1016/S1388-2481(02)00555-6.
[42] A. Hayashi, S. Kama, F. Mizuno, K. Tadanaga, T. Minami, M. Tatsumisago, Characterization of Li2S-P2S5 glass-ceramics as a solid electrolyte for lithium secondary batteries, Solid State Ionics 175 (2004) 683–686, https://doi.org/10.1016/j.ssi.2004.08.036.
[43] J. Trevey, J.S. Jang, Y.S. Jung, C.R. Stoldt, S.H. Lee, Glass-ceramic Li2S-P2S5 electrolytes prepared by a single step ball billing process and their application for all-solid-state lithium-ion batteries, Electrochem. Commun. 11 (2009) 1830–1833, https://doi.org/10.1016/j.elecom.2009.07.028.
[44] Y. Zhang, R. Chen, T. Liu, Y. Shen, Y. Lin, C.W. Nan, High capacity, superior cyclic performances in all-solid-state lithium-ion batteries based on 78Li2S-22P2S5glass-ceramic electrolytes prepared via simple heat treatment, ACS Appl. Mater. Interfaces 9 (2017) 28542–28548, https://doi.org/10.1021/acsami.7b06038.
[45] H. Tsukasaki, S. Mori, H. Morimoto, A. Hayashi, M. Tatsumisago, Direct observation of a non-crystalline state of Li2S–P2S5 solid electrolytes, Sci. Rep. 7 (2017), https://doi.org/10.1038/s41598-017-04030-y.
[46] S. Choi, S. Lee, J. Park, W.T. Nichols, D. Shin, Facile synthesis of Li2S-P2S5 glass-ceramics electrolyte with micron range particles for all-solid-state batteries via a low-temperature solution technique (LTST), Appl. Surf. Sci. 444 (2018) 10–14, https://doi.org/10.1016/j.apsusc.2018.02.270.
[47] R. Garcia-Mendez, F. Mizuno, R. Zhang, T.S. Arthur, J. Sakamoto, Effect of processing conditions of 75Li2S-25P2S5 solid electrolyte on its DC electrochemical behavior, Electrochim. Acta 237 (2017) 144–151, https://doi.org/10.1016/j.electacta.2017.03.200.
[48] R. Kanno, M. Murayama, Lithium ionic conductor thio-LISICON: the Li2S-GeS2-P2S5 system, J. Electrochem. Soc. 148 (2001) A742, https://doi.org/10.1149/1.1379028.
[49] R. Mercier, J.P. Malugani, B. Fahys, J. Douglande, G. Robert, Synthese, structure cristalline et analyse vibrationnelle de l'hexathiohypodiphosphate de lithium Li4P2S6, J. Solid State Chem. 43 (1982) 151–162, https://doi.org/10.1016/0022-4596(82)90224-9.
[50] R. Mercier, J. Malugani, B. Fahys, R. Guy, Structure du Tetrathiophosphate de Lithium, Acta Crystallogr. B (1982) 1887–1990, https://doi.org/10.1107/S0567740882007535.
[51] K. Homma, M. Yonemura, T. Kobayashi, M. Nagao, M. Hirayama, R. Kanno, Crystal structure and phase transitions of the lithium ionic conductor Li3PS4, Solid State Ionics 182 (2011) 53–58, https://doi.org/10.1016/j.ssi.2010.10.001.
[52] S.T. Kong, Ö. Gün, B. Koch, H.J. Deiseroth, H. Eckert, C. Reiner, Structural characterisation of the Li argyrodites Li7PS6 and Li7PSe6 and their solid solutions: quantification of site preferences by MAS-NMR spectroscopy, Chem. Eur J. 16 (2010) 5138–5147, https://doi.org/10.1002/chem.200903023.
[53] R. Mercier, J.P. Malugani, B. Fahys, G. Robert, Superionic conduction in Li2S-P2S5-Lil-glasses, Solid State Ionics 5 (1981) 663–666.
[54] Z.D. Hood, C. Kates, M. Kirkham, S. Adhikari, C. Liang, N.A.W. Holzwarth, Structural and electrolyte properties of Li4P2S6, Solid State Ionics 284 (2015) 61–70, https://doi.org/10.1016/j.ssi.2015.10.015.
[55] H. Tsukasaki, S. Mori, S. Shiotani, H. Yamamura, Ionic conductivity and crystallization process in the Li2S–P2S5 glass electrolyte, Solid State Ionics 317 (2018) 122–126, https://doi.org/10.1016/j.ssi.2018.01.010.
[56] Y. Seino, T. Ota, K. Takada, A. Hayashi, M. Tatsumisago, A sulphide lithium super ion conductor is superior to liquid ion conductors for use in rechargeable batteries, Energy Environ. Sci. 7 (2014) 627–631, https://doi.org/10.1039/C3EE41655K.
[57] I.H. Chu, H. Nguyen, S. Hy, Y.C. Lin, Z. Wang, Z. Xu, Z. Deng, Y.S. Meng, S.P. Ong, Insights into the performance limits of the Li7P3S11 superionic conductor: a combined first-principles and experimental study, ACS Appl. Mater. Interfaces 8 (2016) 7843–7853, https://doi.org/10.1021/acsami.6b00833.
[58] H. Yamane, M. Shibata, Y. Shimane, T. Junke, Y. Seino, S. Adams, K. Minami, A. Hayashi, M. Tatsumisago, Crystal structure of a superionic conductor, Li7P3S11, Solid State Ionics 178 (2007) 1163–1167, https://doi.org/10.1016/j.ssi.2007.05.020.
[59] Y. Wang, W.D. Richards, S.P. Ong, L.J. Miara, J.C. Kim, Y. Mo, G. Ceder, Design principles for solid-state lithium superionic conductors, Nat. Mater. 14 (2015) 1026–1031, https://doi.org/10.1038/nmat4369.
[60] S. Wenzel, D.A. Weber, T. Leichtweiss, M.R. Busche, J. Sann, J. Janek, Interphase formation and degradation of charge transfer kinetics between a lithium metal anode and highly crystalline Li7P3S11 solid electrolyte, Solid State Ionics 286

(2016) 24–33, https://doi.org/10.1016/j.ssi.2015.11.034.
[61] K. Minami, A. Hayashi, M. Tatsumisago, Crystallization process for superionic Li7P3S11 glass-ceramic electrolytes, J. Am. Ceram. Soc. 94 (2011) 1779–1783, https://doi.org/10.1111/j.1551-2916.2010.04335.x.
[62] M. Calpa, N.C. Rosero Navarro, A. Miura, K. Tadanaga, Preparation of sulfide solid electrolytes in the Li2S-P2S5 system by a liquid phase process, Inorg. Chem. Front. (2018) 501–508, https://doi.org/10.1039/C7QI00737J.
[63] K. Homma, M. Yonemura, M. Nagao, M. Hirayama, R. Kanno, Crystal structure of high-temperature phase of lithium ionic conductor, Li3PS4, J. Phys. Soc. Japan. 79 (2010) 90–93, https://doi.org/10.1143/JPSJS.79SA.90.
[64] S. Iikubo, K. Shimoyama, S. Kawano, M. Fujii, K. Yamamoto, M. Matsushita, T. Shinmei, Y. Higo, H. Ohtani, Novel stable structure of Li3PS4 predicted by evolutionary algorithm under high-pressure, AIP Adv. 8 (2018) 015008, , https://doi.org/10.1063/1.5011401.
[65] M. Murayama, N. Sonoyama, A. Yamada, R. Kanno, Material design of new lithium ionic conductor, thio-LISICON, in the Li2S–P2S5 system, Solid State Ionics 170 (2004) 173–180, https://doi.org/10.1016/j.ssi.2004.02.025.
[66] H. Stöffler, T. Zinkevich, M. Yavuz, A. Senyshyn, J. Kulisch, P. Hartmann, T. Adermann, S. Randau, F.H. Richter, J. Janek, S. Indris, H. Ehrenberg, Li + -ion dynamics in β-Li 3 PS 4 observed by NMR: local hopping and long-range transport, J. Phys. Chem. C 122 (2018) 15954–15965, https://doi.org/10.1021/acs.jpcc.8b05431.
[67] Y. Chen, L. Cai, Z. Liu, C.R. dela Cruz, C. Liang, K. An, Correlation of anisotropy and directional conduction in β-Li3PS4 fast Li+ conductor, Appl. Phys. Lett. 107 (2015) 013904, , https://doi.org/10.1063/1.4926725.
[68] A. Hayashi, S. Hama, H. Morimoto, M. Tatsumisago, T. Minami, Preparation of Li2S–P2S5 amorphous solid electrolytes by mechanical milling, J. Am. Ceram. Soc. 84 (2001) 477–479, https://doi.org/10.1111/j.1151-2916.2001.tb00685.x.
[69] H.-J. Deiseroth, J. Maier, K. Weichert, V. Nickel, S.-T. Kong, C. Reiner, Li7PS6 and Li6PS5X (X: Cl, Br, I): possible three-dimensional diffusion pathways for lithium ions and temperature dependence of the ionic conductivity by impedance measurements, Z. Anorg. Allg. Chem. 637 (2011) 1287–1294, https://doi.org/10.1002/zaac.201100158.
[70] H.J. Deiseroth, J. Maier, K. Weichert, V. Nickel, S.T. Kong, C. Reiner, Li7PS6 and Li6PS5X (X: Cl, Br, I): possible three-dimensional diffusion pathways for lithium ions and temperature dependence of the ionic conductivity by impedance measurements, Z. Anorg. Allg. Chem. 637 (2011) 1287–1294, https://doi.org/10.1002/zaac.201100158.
[71] M. Otoyama, A. Sakuda, A. Hayashi, M. Tatsumisago, Optical microscopic observation of graphite composite negative electrodes in all-solid-state lithium batteries, Solid State Ionics 323 (2018) 123–129, https://doi.org/10.1016/j.ssi.2018.04.023.
[72] M. Pan, T. Hakari, A. Sakuda, A. Hayashi, Y. Suginaka, S. Mori, M. Tatsumisago, Electrochemical properties of all-solid-state lithium batteries with amorphous fesx-based composite positive electrodes prepared via mechanochemistry, Electrochemistry 86 (4) (2018) 175–178 https://doi.org/10.5796/electrochemistry.17-00104.
[73] A. Hayashi, K. Minami, S. Ujiie, M. Tatsumisago, Preparation and ionic conductivity of Li7P3S11 − z glass-ceramic electrolytes, J. Non-Cryst. Solids 356 (2010) 2670–2673, https://doi.org/10.1016/j.jnoncrysol.2010.04.048.
[74] K.H. Park, Q. Bai, D.H. Kim, D.Y. Oh, Y. Zhu, Y. Mo, Y.S. Jung, Design strategies, practical considerations, and new solution processes of sulfide solid electrolytes for all-solid-state batteries, Adv. Energy Mater. 8 (2018) 1800035, https://doi.org/10.1002/aenm.201800035.
[75] Z.D. Hood, H. Wang, A.S. Pandian, R. Peng, K.D. Gilroy, M. Chi, C. Liang, Y. Xia, Fabrication of sub-micrometer-thick solid electrolyte membranes of β-Li 3 PS 4 via tiled assembly of nanoscale, plate-like building blocks, Adv. Energy Mater. (2018) 1800014, , https://doi.org/10.1002/aenm.201800014.
[76] H.-D. Lim, X. Yue, X. Xing, V. Petrova, M. Gonzalez, H. Liu, ping liu, Designing solution chemistries for low-temperature synthesis of sulfide-based solid electrolytes, J. Mater. Chem. A (2018), https://doi.org/10.1039/C8TA01800F.
[77] Y. Wang, D. Lu, M. Bowden, P.Z. El Khoury, K.S. Han, Z.D. Deng, J. Xiao, J.-G. Zhang, J. Liu, Mechanism of formation of Li 7 P 3 S 11 solid electrolytes through liquid phase synthesis, Chem. Mater. 30 (2018) 990–997, https://doi.org/10.1021/acs.chemmater.7b04842.
[78] M. Calpa, N.C. Rosero Navarro, A. Miura, K. Tadanaga, Preparation of sulfide solid electrolytes in the Li $_2$ S-P $_2$ S $_5$ system by a liquid phase process, Inorg. Chem. Front. (2017), https://doi.org/10.1039/C7QI00737J.
[79] M. Calpa, N.C. Rosero-Navarro, A. Miura, K. Tadanaga, Instantaneous preparation of high lithium-ion conducting sulfide solid electrolyte Li $_7$ P $_3$ S $_{11}$ by a liquid phase process, RSC Adv. 7 (2017) 46499–46504, https://doi.org/10.1039/C7RA09081A.
[80] H. Wang, Z.D. Hood, Y. Xia, C. Liang, Fabrication of ultrathin solid electrolyte membranes of β-Li3PS4 nanoflakes by evaporation-induced self-assembly for all-solid-state batteries, J. Mater. Chem. A. 4 (2016) 8091–8096, https://doi.org/10.1039/C6TA02294D.
[81] A. Matsuda, H. Muto, N.H.H. Phuc, Preparation of Li3PS4 solid electrolyte by liquid-phase shaking using organic solvents with carbonyl group as complex forming medium, J. Jpn. Soc. Powder Powder Metall. 63 (2016) 976–980, https://doi.org/10.2497/jjspm.63.976.
[82] S.J. Sedlmaier, S. Indris, C. Dietrich, M. Yavuz, C. Dräger, F. von Seggern, H. Sommer, J. Janek, Li 4 PS 4 I: a Li + superionic conductor synthesized by a solvent-based soft chemistry approach, Chem. Mater. 29 (2017) 1830–1835, https://doi.org/10.1021/acs.chemmater.7b00013.
[83] H.-D. Lim, X. Yue, X. Xing, V. Petrova, M. Gonzalez, H. Liu, P. Liu, Designing solution chemistries for low-temperature synthesis of sulfide-based solid electrolytes, J. Mater. Chem. A (2018), https://doi.org/10.1039/C8TA01800F.
[84] S. Ito, M. Nakakita, Y. Aihara, T. Uehara, N. Machida, A synthesis of crystalline Li7P3S11 solid electrolyte from 1,2-dimethoxyethane solvent, J. Power Sources 271 (2014) 342–345, https://doi.org/10.1016/j.jpowsour.2014.08.024.
[85] N.H.H. Phuc, K. Morikawa, M. Totani, H. Muto, A. Matsuda, Chemical synthesis of Li3PS4 precursor suspension by liquid-phase shaking, Solid State Ionics 285 (2016) 2–5, https://doi.org/10.1016/j.ssi.2015.11.019.
[86] H.-D. Lim, H.-K. Lim, X. Xing, B.-S. Lee, H. Liu, C. Coaty, H. Kim, P. Liu, Solid electrolyte layers by solution deposition, Adv. Mater. Interfaces (2018) 1701328, , https://doi.org/10.1002/admi.201701328.
[87] Y. Lu, S. Gu, X. Hong, K. Rui, X. Huang, J. Jin, C. Chen, J. Yang, Z. Wen, Pre-modified Li 3 PS 4 based interphase for lithium anode towards high-performance Li-S battery, Energy Storage Mater (2017), https://doi.org/10.1016/j.ensm.2017.09.007.
[88] Q. Pang, X. Liang, A. Shyamsunder, L.F. Nazar, An in vivo formed solid electrolyte surface layer enables stable plating of Li metal, Joule (2017) 1–16, https://doi.org/10.1016/j.joule.2017.11.009.
[89] S. Teragawa, K. Aso, K. Tadanaga, A. Hayashi, M. Tatsumisago, Liquid-phase synthesis of a Li3PS4 solid electrolyte using N-methylformamide for all-solid-state lithium batteries, J. Mater. Chem. A. 2 (2014) 5095, https://doi.org/10.1039/c3ta15090a.
[90] N.H.H. Phuc, K. Morikawa, M. Totani, H. Muto, A. Matsuda, Chemical synthesis of Li3PS4 precursor suspension by liquid-phase shaking, Solid State Ionics 285 (2016) 2–5, https://doi.org/10.1016/j.ssi.2015.11.019.
[91] H. Muramatsu, A. Hayashi, T. Ohtomo, S. Hama, M. Tatsumisago, Structural change of Li2S-P2S5 sulfide solid electrolytes in the atmosphere, Solid State Ionics 182 (2011) 116–119, https://doi.org/10.1016/j.ssi.2010.10.013.
[92] T. Hakari, M. Deguchi, K. Mitsuhara, T. Ohta, K. Saito, Y. Orikasa, Y. Uchimoto, Y. Kowada, A. Hayashi, M. Tatsumisago, Structural and Electronic State Changes of a Sulfide Solid Electrolyte during the Li Deinsertion/Insertion Processes, (2017), https://doi.org/10.1021/acs.chemmater.7b00551.
[93] K.N. Wood, K.X. Steirer, S.E. Hafner, C. Ban, S. Santhanagopalan, G. Teeter, N. Renewable, Operando X-ray photoelectron spectroscopy of solid electrolyte interphase formation and evolution in Li2S-P2S5 solid-state electrolytes, Nat. Commun. 9 (1) (2018) 2490, https://doi.org/10.1038/s41467-018-04762-z.
[94] B.R. Shin, Y.J. Nam, D.Y. Oh, D.H. Kim, J.W. Kim, Y.S. Jung, Comparative study of TiS2/Li-in all-solid-state lithium batteries using glass-ceramic Li3PS4 and Li10GeP2S12 solid electrolytes, Electrochim. Acta 146 (2014) 395–402, https://doi.org/10.1016/j.electacta.2014.08.139.
[95] A. Cassel, B. Fleutot, M. Courty, V. Viallet, M. Morcrette, Sol-gel synthesis and electrochemical properties extracted by phase inflection detection method of NASICON-type solid electrolytes LiZr2(PO4)3and Li1.2Zr1.9Ca0.1(PO4)3, Solid State Ionics 309 (2017) 63–70, https://doi.org/10.1016/j.ssi.2017.07.009.
[96] J. Nguyen, B. Fleutot, R. Janot, Investigation of the stability of metal borohydrides-based compounds LiM(BH4)3Cl (M = La, Ce, Gd) as solid electrolytes for Li-S batteries, Solid State Ionics 315 (2018) 26–32, https://doi.org/10.1016/j.ssi.2017.11.033.